Supplementary information

Confined flash printing and synthesis of stable perovskite nanofilms under ambient conditions

Yuxin Liu, Tanja Knaus, Zheng Wei, Junfang Zhang, Matteo Damian, Sebastian Ronneberger, Xingjun Zhu, Peter H. Seeberger, Hong Zhang, Francesco G. Mutti, and Felix F. Loeffler

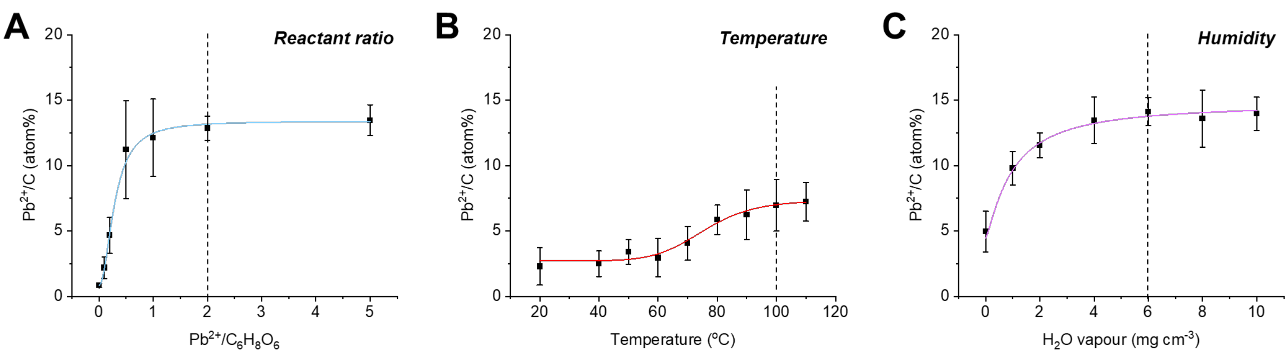

Figure S1. Optimization of parameters for Pb^{2+}-alginate hydrogel formation on a substrate. The fixation efficiency of Pb^{2+} on substrate with different (A) reactant ratio, (B) temperature, and (C) humidity was analyzed.

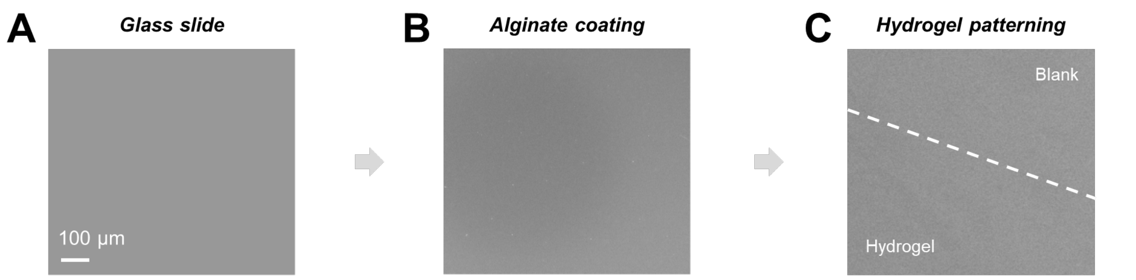

	Glass
C%	1.4 ± 1.2
Pb%	-

	Alginate
C%	13.6 ± 2.7
Pb%	-

	Blank	Hydrogel
C%	12.4 ± 1.3	12.2 ± 1.8
Pb%	0.2 ± 0.3	2.5 ± 1.1

Figure S2. Characterization of Pb^{2+}-alginate hydrogel modified glass slide. (A) Scanning electron microscopy image and energy-dispersive X-ray analysis of cleaned glass slide, (B) glass slide coated with alginate, and (C) glass slide modified with Pb^{2+}-alginate hydrogel. The hydrogel and blank background were outlined by a dashed line, based on the Pb^{2+} distribution.

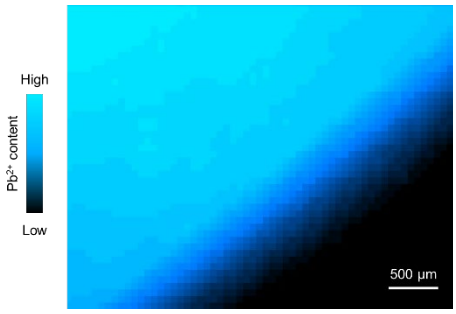

Figure S3. Quantitative elemental mapping of a Pb^{2+}-alginate hydrogel film on the edge of a transferred and reacted PEG-Pb pattern.

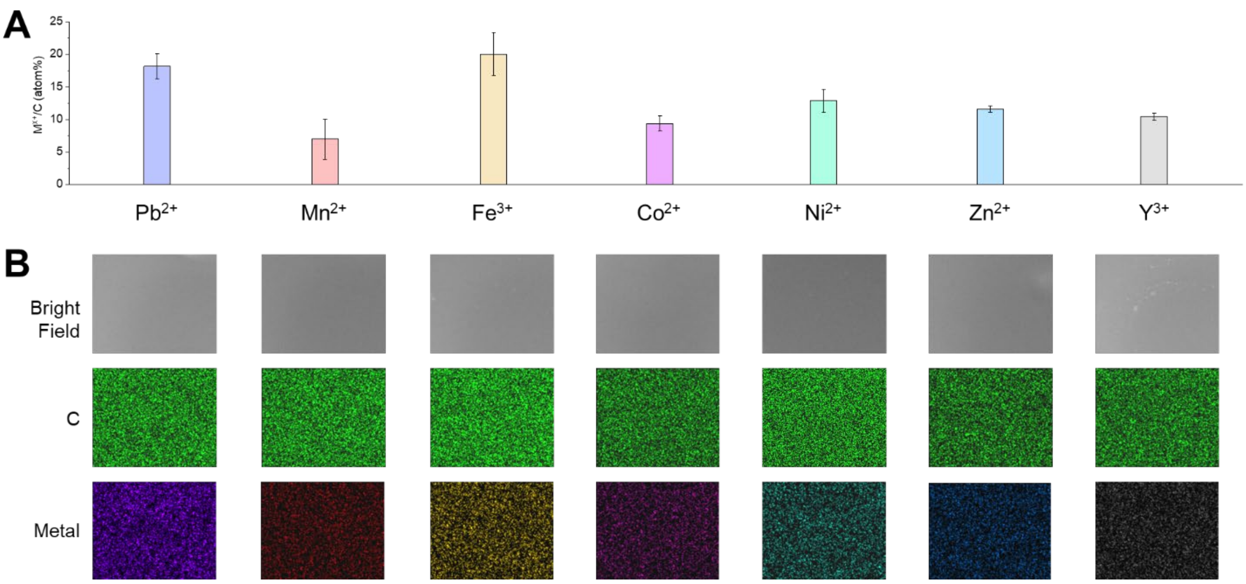

Figure S4. Formation of alginate hydrogels with different metal ions. (A) M^{x+}/C ratio, (B) scanning electron microscope and energy-dispersive X-ray analysis elemental mapping profile of the hydrogel formed by using different metal ions, including Pb^{2+}, Mn^{2+}, Fe^{3+}, Co^{2+}, Ni^{2+}, Zn^{2+}, and Y^{3+}.

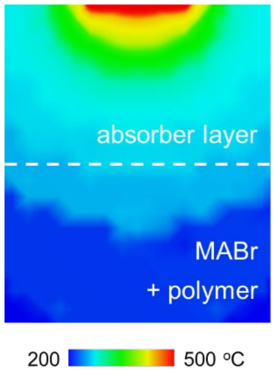

Figure S5. Temperature distribution during the conFlash synthesis. Finite element simulation of the heat conduction from the absorber layer to the polymer layer containing the methylammonium bromide (MABr) precursor.

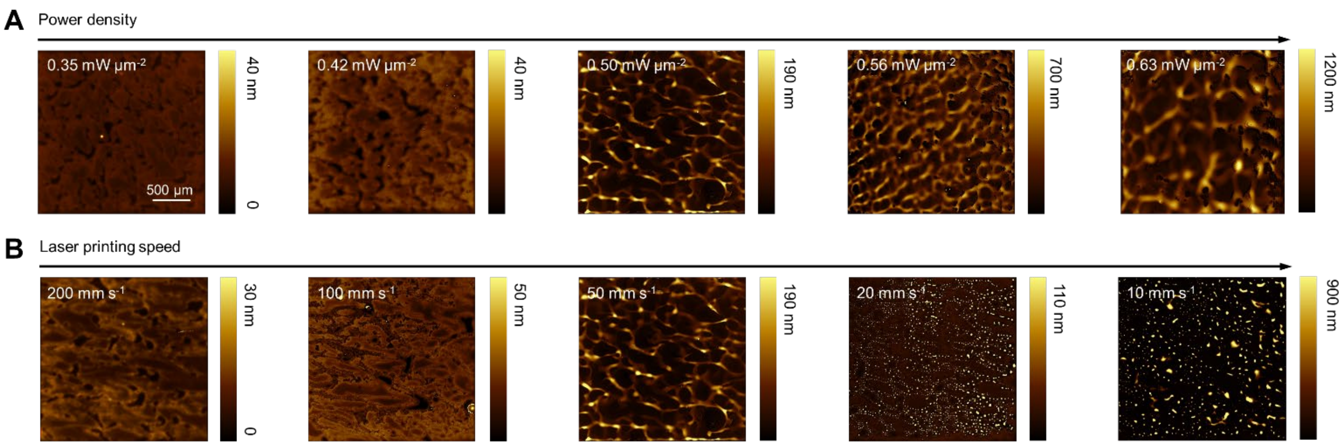

Figure S6. Morphology of nanofilm generated by different laser parameters. (A) Vertical scanning interferometry height measurement of PQD nanofilms on a glass slide, prepared by relative laser power densities of 0.35 – 0.63 mW μm^{-2} with a printing speed of 50 mm s^{-1} and (B) by laser printing speeds of 200 – 10 mm s^{-1} with a relative laser power density of 0.50 mW μm^{-2}.

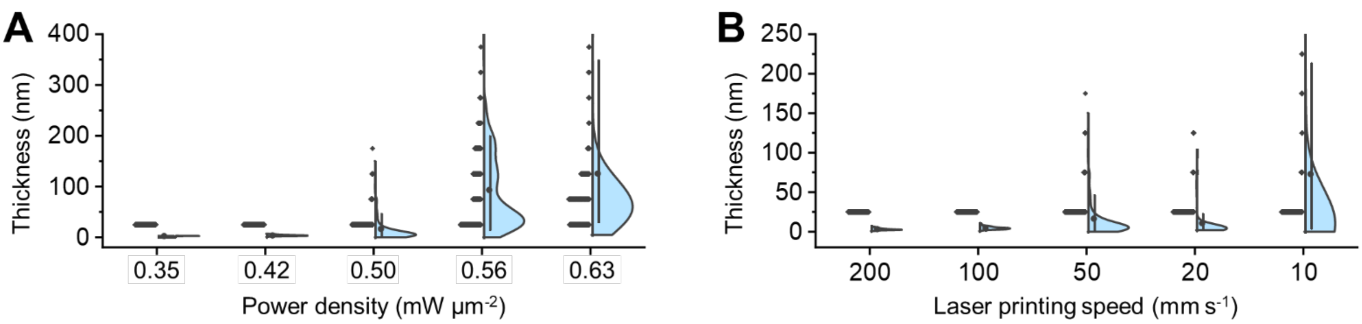

Figure S7. Thickness of nanofilm generated by different laser parameters. Thickness distribution of PQD nanofilms on a glass slide, (A) prepared by relative laser power densities of 0.35 – 0.63 mW μm^{-2} with a printing speed of 50 mm s^{-1} and (B) by laser printing speeds of 200 – 10 mm s^{-1} with a relative laser power density of 0.50 mW μm^{-2}.

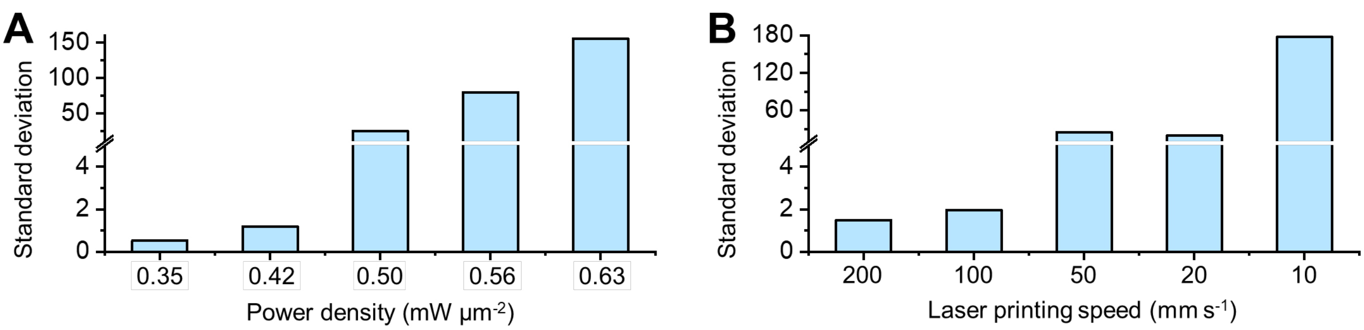

Figure S8. Flatness of nanofilm generated by different laser parameters. Standard deviation of thickness of PQD nanofilms on a glass slide, (A) prepared by relative laser power densities of 0.35 – 0.63 mW μm^{-2}

with a printing speed of 50 mm s^{-1} and (B) by laser printing speeds of 200 – 10 mm s^{-1} with a relative laser power density of 0.50 mW μm^{-2}.

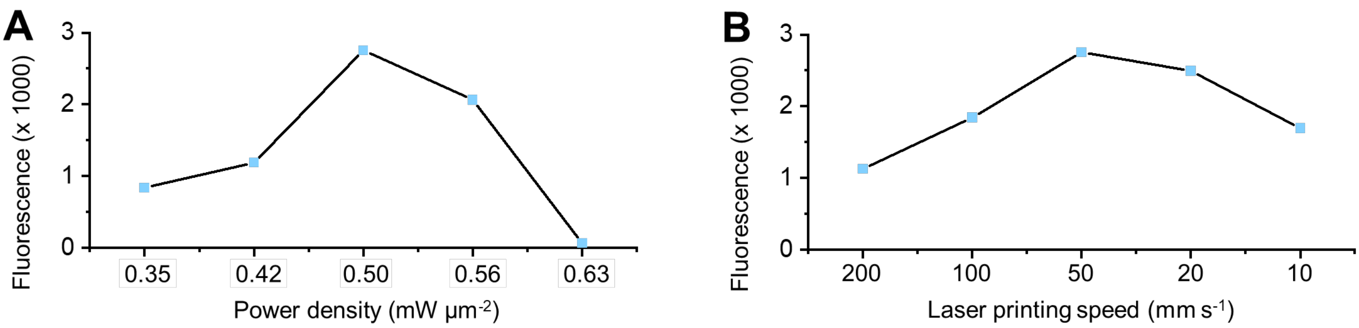

Figure S9. Fluorescence of nanofilm generated by different laser parameters. Fluorescence intensity of PQD nanofilms on a glass slide, (A) prepared by relative laser power densities of 0.35 – 0.63 mW μm^{-2} with a printing speed of 50 mm s^{-1} and (B) by laser printing speeds of 200 – 10 mm s^{-1} with a relative laser power density of 0.50 mW μm^{-2}.

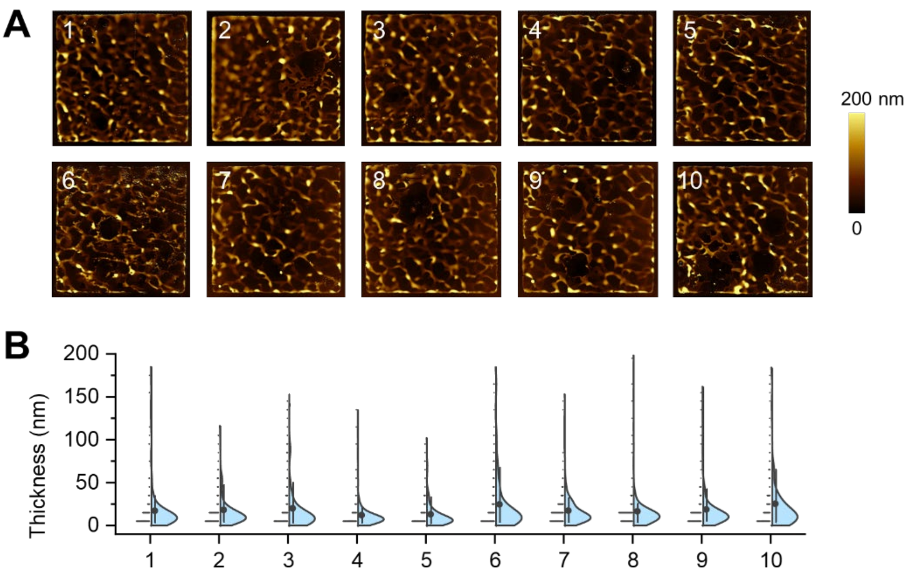

Figure S10. Thickness profile of the PQD nanofilms. (A) VSI measurement and (B) thickness distribution of 10 different PQD nanofilms on a glass slide.

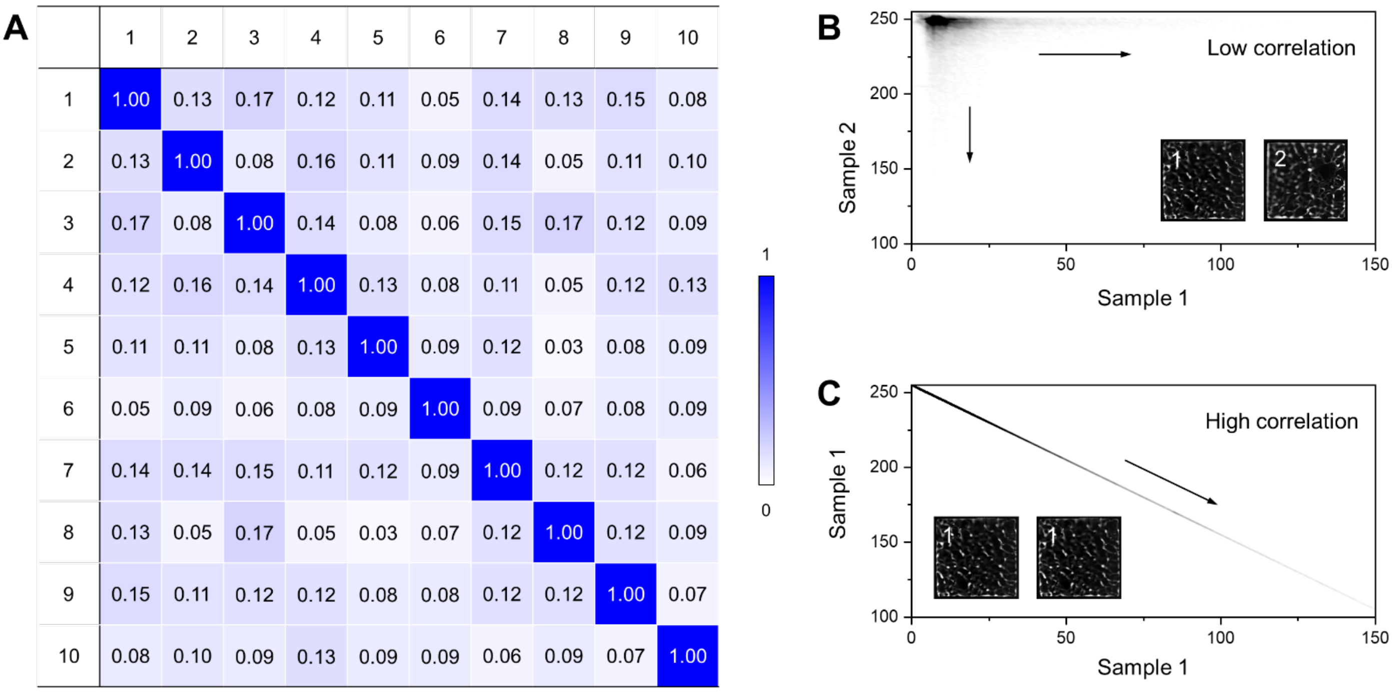

	1	2	3	4	5	6	7	8	9	10
1	1.00	0.13	0.17	0.12	0.11	0.05	0.14	0.13	0.15	0.08
2	0.13	1.00	0.08	0.16	0.11	0.09	0.14	0.05	0.11	0.10
3	0.17	0.08	1.00	0.14	0.08	0.06	0.15	0.17	0.12	0.09
4	0.12	0.16	0.14	1.00	0.13	0.08	0.11	0.05	0.12	0.13
5	0.11	0.11	0.08	0.13	1.00	0.09	0.12	0.03	0.08	0.09
6	0.05	0.09	0.06	0.08	0.09	1.00	0.09	0.07	0.08	0.09
7	0.14	0.14	0.15	0.11	0.12	0.09	1.00	0.12	0.12	0.06
8	0.13	0.05	0.17	0.05	0.03	0.07	0.12	1.00	0.12	0.09
9	0.15	0.11	0.12	0.12	0.08	0.08	0.12	0.12	1.00	0.07
10	0.08	0.10	0.09	0.13	0.09	0.09	0.06	0.09	0.07	1.00

Figure S11. Unique microstructure of the PQD nanofilms. (A) Pearson correlation analysis of 10 different PQD nanofilms on a glass slide. Colocalization results of (B) two different PQD nanofilms and (C) the same PQD nanofilm.

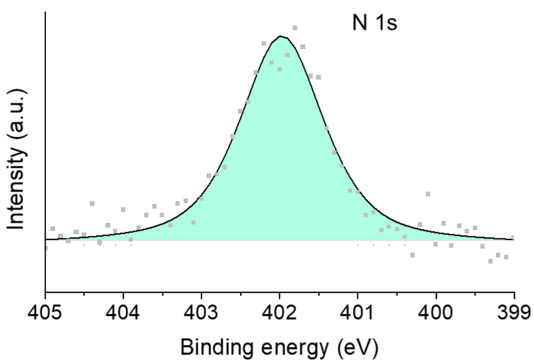

Figure S12. N 1s X-ray photoelectron spectrum of a PQD nanofilm on a glass slide.

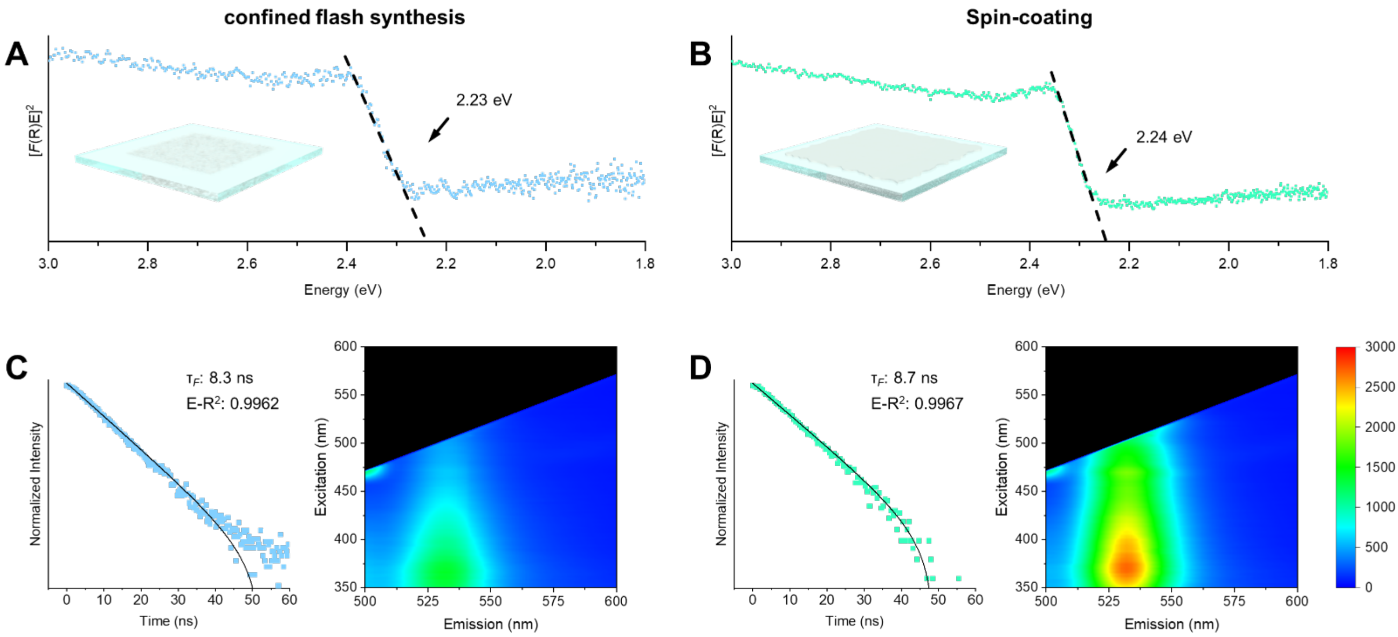

Figure S13. Optical properties of the PQD nanofilm. UV-vis-NIR diffuse reflectance spectrum of a solid stationary sample of $MAPbBr_3$ QD film prepared by (A) our conFlash synthesis method and (B) the spin-coating of pre-synthesized PQDs. The fluorescence life time and 2D fluorescence spectra of $MAPbBr_3$ QDs film prepared by (C) our conFlash synthesis method and (D) the spin-coating of pre-synthesized PQDs. Curves were fitted by the double exponential function, based on the value of E-R^2.

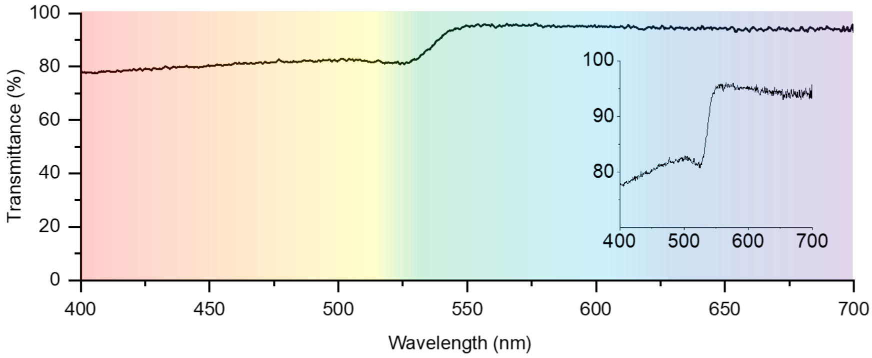

Figure S14. UV-vis-NIR transmittance spectrum of a solid stationary sample of $MAPbBr_3$ QDs film prepared by standard spin-coating method of pre-synthesized PQDs.

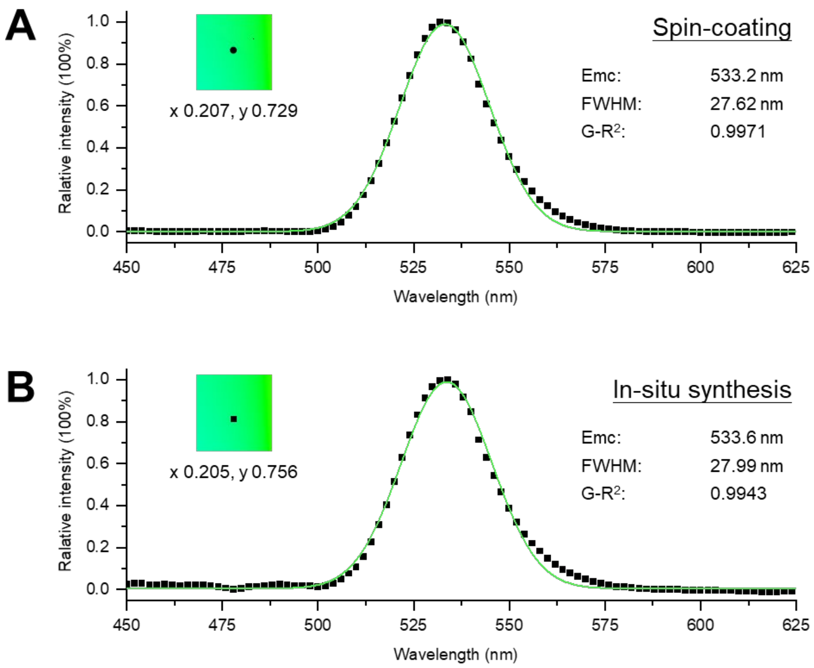

Figure S15. Fluorescence spectra of a solid stationary sample of $MAPbBr_3$ QD film (A) prepared by standard spin-coating method and (B) our confined flash synthesis method under 365 nm excitation. The color coordinates were calculated and inserted according to the Commission internationale de l'éclairage (CIE) standard.

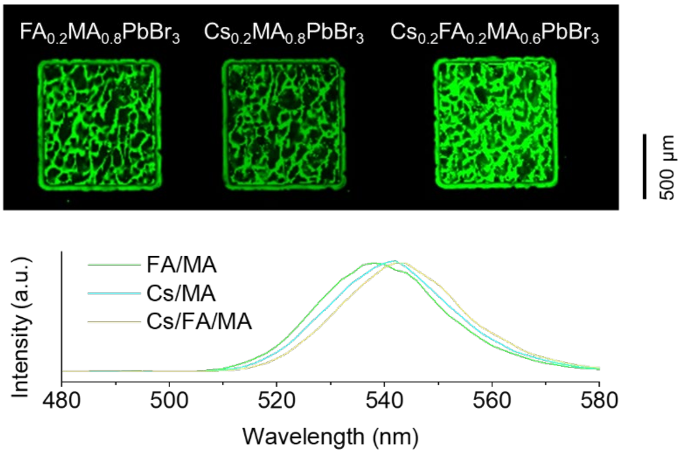

Figure S16. Fluorescence image and fluorescence spectra of $FA_{0.2}MA_{0.8}PbBr_3$, $Cs_{0.2}MA_{0.8}PbBr_3$, and $Cs_{0.2}FA_{0.2}MA_{0.6}PbBr_3$ on a glass substrate.

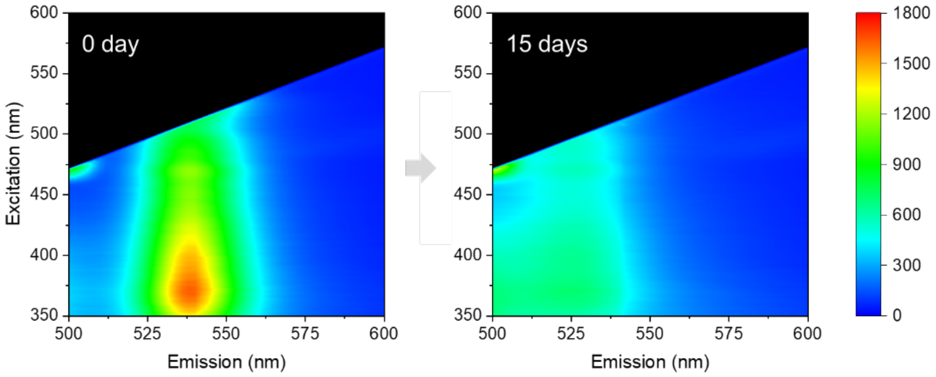

Figure S17. 2D fluorescence spectra of $MAPbBr_3$ QDs film without polymer coating freshly prepared by standard spin-coating method and after 15 days standing.

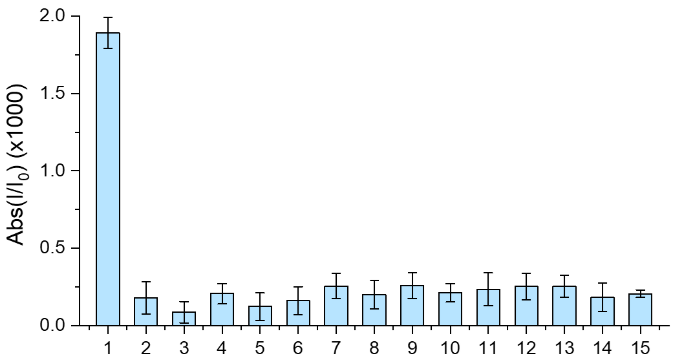

Figure S18. Selectivity test of (1) H_2O_2 (10 μM) detection toward (2) Na^+, (3) K^+, (4) Mg^{2+}, (5) Ca^{2+}, (6) Cl^-,

(7) PO_4^{3-}, (8) uridine, (9) phospholipid, (10) glycine, (11) glucose, (12) ascorbic acid, (13), dopamine, (14) reduced glutathione, and (15) human serum albumin (1 mM).

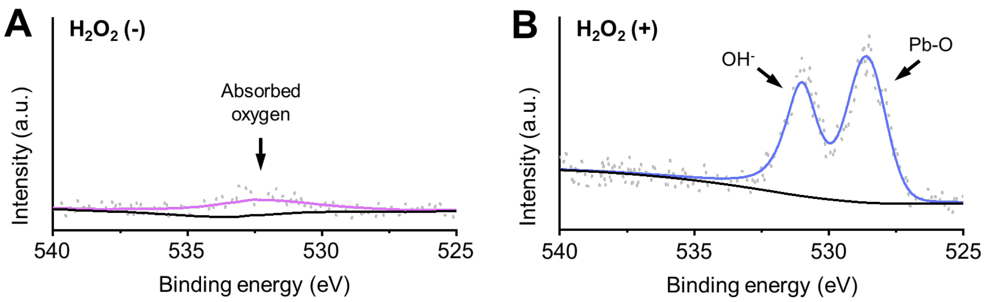

Figure S19. O 1s X-ray photoelectron spectrum of a PQD nanofilm on a Si slide before (A) and after reaction with H_2O_2 (B).

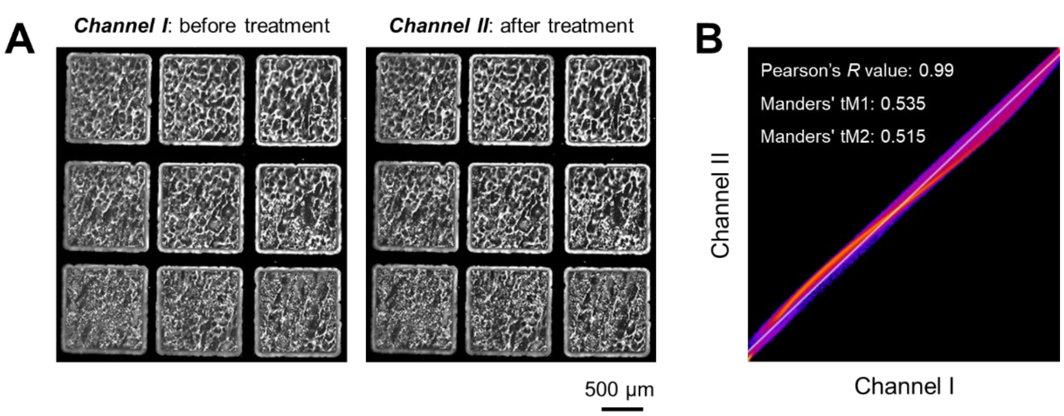

Figure S20. (A) Fluorescence images of nine patterns of a PQD nanofilm before and after 30 min rinsing treatment. (B) 2D intensity histogram of the colocalization between signal of channel I and channel II.

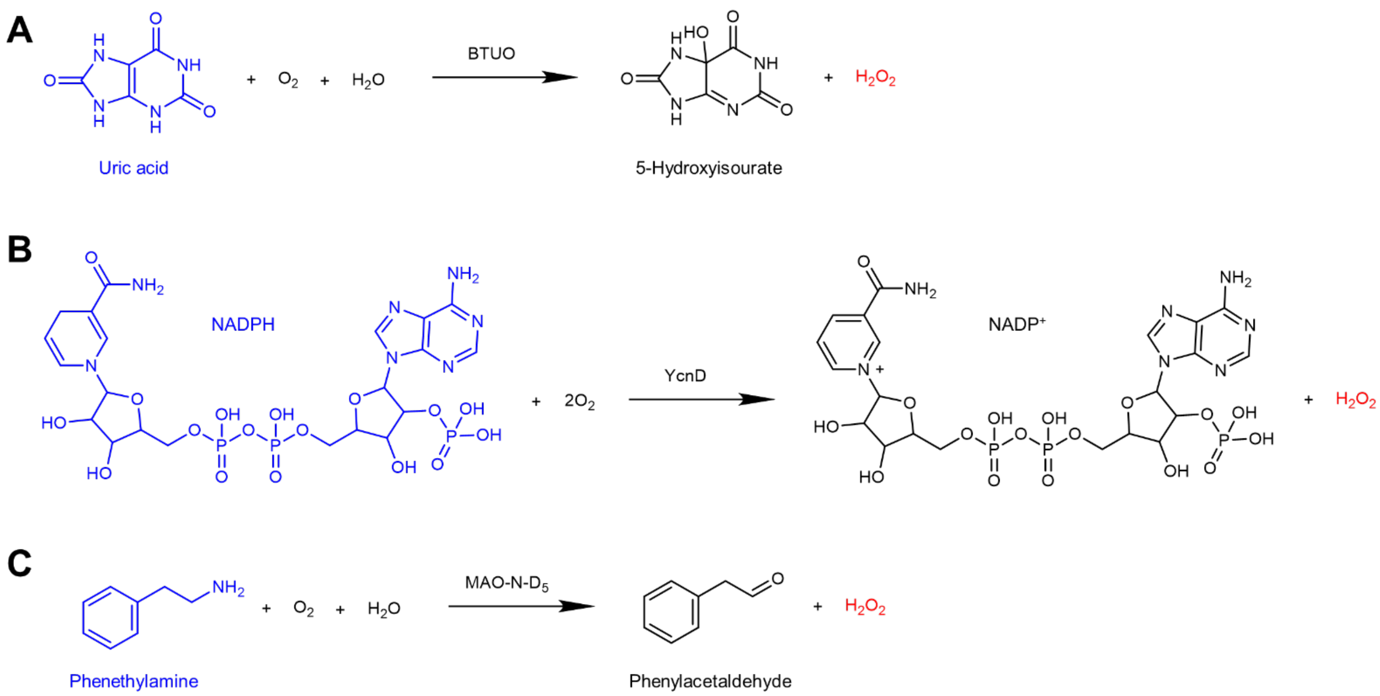

Figure S21. Oxidation of (A) uric acid, (B) NADPH, and (C) phenethylamine by engineered *Bacillus sp.* TB-90 urate oxidase (BTUO), *Bacillus sp.* flavin-containing NADPH oxidoreductase (YcnD), and *Aspergillus niger* monoamine oxidase (MAO-N-D5), respectively. The target analytes were highlighted in blue, while the produced H_2O_2 by the oxidation process was highlighted in red.

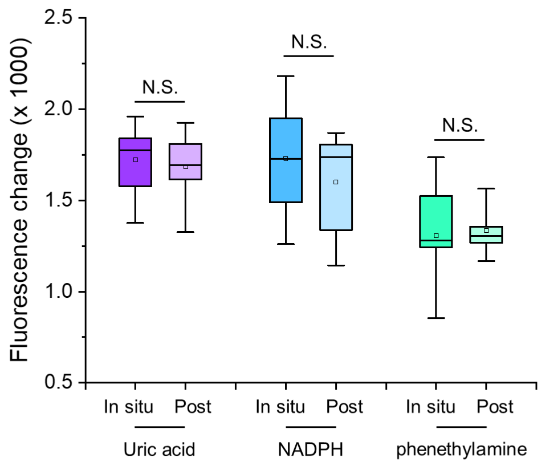

Figure S22. Fluorescence change of enzyme-modified PQD nanofilms (n = 9) responding to uric acid, NADPH, and phenethylamine (In situ, darker color) and PQD nanofilms responding to enzymatic oxidation products of uric acid, NADPH, and phenethylamine (Post, pale color). Center line, median; square, mean; box limits, upper and lower quartiles; whiskers, 1.5× interquartile range. Statistical significance was determined by one-way t-tests. N.S. is not significant.

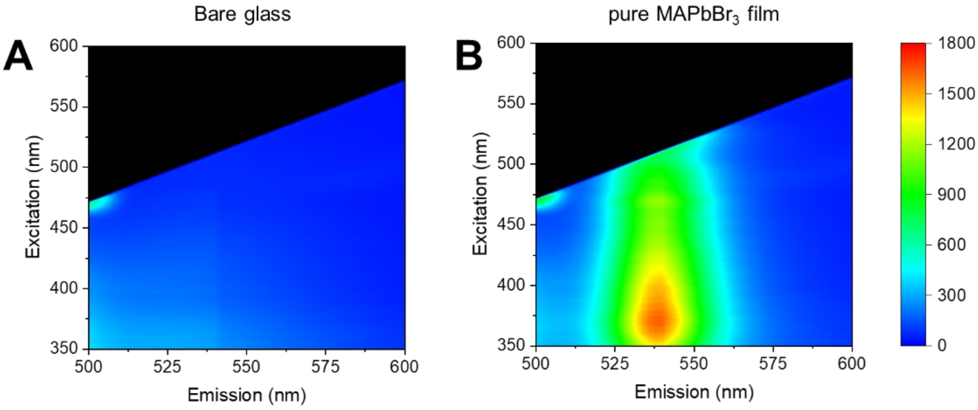

Figure S23. 2D fluorescence spectra of (A) bare glass slide and (B) $MAPbBr_3$ QDs film with polymer coating prepared by pre-synthesis and standard spin-coating method.